Cellular and Molecular Life Sciences (2021) 78:1565–1575
https://doi.org/10.1007/s00018-020-03592-x

ORIGINAL ARTICLE

NACHO and 14-3-3 promote expression of distinct subunit stoichiometries of the α4β2 acetylcholine receptor

Simone Mazzaferro[1] · Sara T. Whiteman[2] · Constanza Alcaino[2] · Arthur Beyder[1,2] · Steven M. Sine[1,3,4]

Received: 10 April 2020 / Revised: 19 June 2020 / Accepted: 1 July 2020 / Published online: 16 July 2020
© Springer Nature Switzerland AG 2020

Abstract

Nicotinic acetylcholine receptors (nAChRs) belong to the superfamily of pentameric ligand-gated ion channels, and in neuronal tissues, are assembled from various types of α- and β-subunits. Furthermore, the subunits α4 and β2 assemble in two predominant stoichiometric forms, $(\alpha4)_2(\beta2)_3$ and $(\alpha4)_3(\beta2)_2$, forming receptors with dramatically different sensitivity to agonists and allosteric modulators. However, mechanisms by which the two stoichiometric forms are regulated are not known. Here, using heterologous expression in mammalian cells, single-channel patch-clamp electrophysiology, and calcium imaging, we show that the ER-resident protein NACHO selectively promotes the expression of the $(\alpha4)_2(\beta2)_3$ stoichiometry, whereas the cytosolic molecular chaperone 14-3-3η selectively promotes the expression of the $(\alpha4)_3(\beta2)_2$ stoichiometry. Thus, NACHO and 14-3-3η are potential physiological regulators of subunit stoichiometry, and are potential drug targets for re-balancing the stoichiometry in pathological conditions involving α4β2 nAChRs such as nicotine dependence and epilepsy.

Keywords Ligand-gated ion channels · Neurotransmitters · Nicotine addiction · Chaperones

Introduction

Nicotinic acetylcholine receptors (nAChRs) are ligand-gated ion channels that mediate rapid excitatory synaptic transmission in the central and peripheral nervous systems [1, 2]. They participate in a wide variety of physiological processes, including skeletal muscle contraction, neurosecretion and synaptic plasticity [3–6]. nAChRs also contribute to higher-order processes such as cognition, working memory, attention, and reward [7–11]. Dysfunction of nAChRs contributes to epilepsy, schizophrenia, neurodegenerative diseases, and nicotine addiction [2, 12–15]. nAChRs belong to the superfamily of pentameric ligand-gated ion channels, and in mammalian neuronal tissues, are assembled from various combinations of eight types of α-subunits and three types of β-subunits. This combinatorial assembly is significant because the types, stoichiometry, and positioning of subunits determine the function and pharmacology of the pentameric unit [1, 16]. For example, the α4β2 nAChR, the most abundant type of nicotinic receptor in the brain [17–20], assembles in two predominant stoichiometric forms, $(\alpha4)_2(\beta2)_3$ and $(\alpha4)_3(\beta2)_2$, which differ dramatically in their sensitivity to agonists and allosteric modulators [21–28]. In heterologous expression systems, biasing the ratio of cDNAs encoding α4 and β2 subunits is often used to produce a receptor population enriched in a single stoichiometric form [25, 26, 29]. Also, small exogenous molecules such as nicotine or its metabolite cotinine act as intracellular chaperones to bias the receptor population toward a single stoichiometric form [21, 25, 30–35]. However, cellular mechanisms that regulate the balance of the stoichiometric forms of nAChRs are largely unexplored.

✉ Simone Mazzaferro
Mazzaferro.Simone@mayo.edu

✉ Sara T. Whiteman
whiteman.sara@gmail.com

Steven M. Sine
sine@mayo.edu

1 Department of Physiology and Biomedical Engineering, Mayo Clinic College of Medicine, Rochester, MN 55905, USA

2 Enteric Neuroscience Program (ENSP), Division of Gastroenterology & Hepatology, Department of Medicine, Mayo Clinic, Rochester, MN 55905, USA

3 Department of Neurology, Mayo Clinic College of Medicine, Rochester, MN 55905, USA

4 Department of Molecular Pharmacology and Experimental Therapeutics, Mayo Clinic College of Medicine, Rochester, MN 55905, USA

Recently the ER-resident protein NACHO was shown to increase trafficking of several types of nAChRs to the plasma membrane, including the homomeric α7 and the heteromeric α4β2, α3β2 and α3β4 nAChRs [36–38]. NACHO is highly expressed in the central nervous system, and in primary cultures of hippocampal neurons, siRNA targeted against NACHO reduced ACh-elicited whole-cell currents [37]. However, whether NACHO affects the subunit stoichiometry of heteromeric nAChRs has not been investigated.

The 14-3-3 protein family comprises ~ 1% of the total soluble protein in the central nervous system [39], and the subtype 14-3-3η is expressed predominantly in the cerebral cortex [40, 41]. In vitro, 14-3-3η increases expression of α4β2 nAChRs [42], and decreases ACh sensitivity of the resulting nAChRs [43]. Whether the decreased ACh sensitivity arose through a change in the functional state of the α4β2 nAChR or a change in subunit stoichiometry [43], has not been distinguished.

To investigate whether NACHO and 14-3-3η affect the subunit stoichiometry of functional α4β2 nAChRs, we transfected human α4 and β2 subunits into clonal mammalian cells, without or with either NACHO or 14-3-3η. We then used single-channel patch-clamp recording and fluorescence imaging of intracellular Ca^{2+} to assess the subunit stoichiometry of functional α4β2 nAChRs. The results reveal that NACHO and 14-3-3η exert opposing effects on the subunit stoichiometry of functional α4β2 nAChRs. NACHO and 14-3-3η thus emerge as potential physiological regulators of subunit stoichiometry, as well as potential drug targets for re-balancing the subunit stoichiometry in pathological conditions involving α4β2 nAChRs.

Materials and methods

Expression of human α4β2 nAChRs

cDNAs encoding the human α4 and β2 subunits and the protein 14-3-3η were individually sub-cloned into a modified pCI mammalian expression vector (Promega), as previously described [27, 44]. A cDNA encoding the protein NACHO was synthesized by GenScript and sub-cloned into the mammalian expression vector pRBG4 [45]. BOSC 23 cells, a cell line derived from the HEK 293 cell line [46], were maintained in Dulbecco's modified Eagle's medium (DMEM, Gibco) containing 10% fetal bovine serum, and transfected by calcium phosphate precipitation, as previously described [47–49]. For each 35 mm plate of cells, the following quantities of cDNAs were transfected: α4 + β2 ratio 1:1 (3 μg α4 + 3 μg β2); α4 + β2 + NACHO ratio 1:1:0.3 (3 μg α4 + 3 μg β2 + 1 μg NACHO); α4 + β2 + 1433η ratio 1:1:1 (3 μg α4 + 3 μg β2 +3 μg 1433η); α4 + β2 + 1433η ratio 10:1:10 (6 μg α4 + 0.6 μg β2 + 6 μg 1433η). For patch-clamp experiments, a cDNA encoding green fluorescent protein was included in all transfections, whereas for calcium imaging experiments, a cDNA encoding the calcium sensor GCaMP5G (1 μg/μl, Addgene #31788) was included. Transfections were carried out for 4 to 6 h, followed by the medium exchange. Single-channel recordings and calcium imaging experiments were done 48–72 h post-transfection.

Drugs

Nicotine and acetylcholine (ACh) were purchased from Sigma-Aldrich (St Louis, MO, USA), and 3-[3-(3-Pyridinyl)-1,2,4-oxadiazol-5-yl]benzonitrile (NS9283) from Tocris (UK).

Patch-clamp recordings and analysis

Single-channel recordings were obtained in the cell-attached patch configuration at a membrane potential of − 70 mV and a temperature of 23 °C, as previously described [26, 49]. For both patch-clamp and calcium imaging experiments, the extracellular bath solution contained (mM): 142 KCl, 5.4 NaCl, 1.8 $CaCl_2$, 1.7 $MgCl_2$, and 10 HEPES, adjusted to pH 7.4 with NaOH. The solution within the patch pipette contained (mM): 80 KF, 20 KCl, 40 K-aspartate, 2 $MgCl_2$, 1 EGTA, 10 HEPES, adjusted to pH 7.4 with KOH [50, 51]. Concentrated stock solutions of ACh were made in patch pipette solution and stored at − 80 °C until the day of each experiment. Patch pipettes were pulled from glass capillary tubes (No.7052, King Precision Glass) and coated with Sylgard (Dow Corning).

Single-channel currents were recorded using an Axopatch 200B patch-clamp amplifier (Molecular Devices), with the gain set at 100 mV/pA and the cut-off frequency of the internal Bessel filter at 10 kHz. Continuous stretches of single-channel currents were sampled at intervals of 20 μs using a PCI-6111E acquisition card (National Instruments), and recorded to hard disk using the program Acquire (Bruxton Corporation). The current amplitude of each single-channel opening event was detected using the variable amplitude option within TAC 4.2.0 software (Bruxton Corporation), as previously described [26]. The detected amplitudes were entered into histogram bins, and the histograms were fitted by one or two Gaussian functions by maximum likelihood using the program TACFit 4.2.0 [52], yielding the mean, standard deviation, and fractional area for each component. An unpaired *t* test with the Welch correction was used to determine whether the fitted mean current amplitudes and fractional areas for the two Gaussian components were

different from each other, or different across experiments done under the same experimental conditions. Parameters were considered different if the p-value was less than 0.05.

Calcium imaging and analysis

Transfected BOSC 23 cells were seeded on MatTek dishes (MatTeK corporation), placed on an inverted Olympus IX70 epifluorescence microscope, and imaged using a 16-bit high-speed ORCA Flash4.0 sCMOS camera (Hamamatsu). Cells were continuously perfused with extracellular bath solution (5 ml/min) using a gravity-driven perfusion system. Transfected cells were identified by GCaMP5G fluorescence using an excitation wavelength of 480-505 nm and an emission wavelength of 525 nm. Images were taken using a 40X objective and acquired at a rate of three frames per second (100 ms exposure/frame) using a CoolLED *p*E-300Ultra illumination system (CoolLED limited, UK) and Metamorph software (Molecular Devices) for acquisition, driven by pClamp 10 software (Molecular Devices). Responses were triggered by 5 s applications of extracellular bath solution containing 1 μM nicotine, either without or with 30 μM NS9283, every 15 min. Concentrated stock solutions of nicotine and NS9283 were stored at -80 °C until the day of each experiment. Due to the limited solubility NS9283 in H_2O, the NS9283 stock solution was prepared in 100% DMSO. All experimental solutions contained an equivalent concentration of DMSO (0.6%). All experiments were performed at room temperature (23 °C).

BOSC 23 cells were perfused with extracellular bath solution containing 1 μM nicotine, and the fluorescence time course was recorded. After a washout period of 15 min, the same cells were perfused with extracellular bath solution containing 1 μM nicotine plus 30 μM NS9283, and a second fluorescence time course was recorded. Each fluorescence time course was exported to Microsoft Excel, and the change in fluorescence intensity as a function of time was expressed as $(F - F_0)/F_0$) or, $\Delta F/F_0$, where F is the total fluorescence and F_0 is the baseline fluorescence. The extent of NS9283 potentiation was defined as the change in fluorescence in response to nicotine plus NS9283 relative to the response to nicotine alone:

$$\text{Extent of potentiation by NS9283} = \left(\left[\frac{\Delta F\text{Nicotine plus NS9283}}{F0} \Big/ \frac{\Delta F\text{Nicotine}}{F0}\right] - 1\right).$$

A paired t test was used to determine whether the difference between $\Delta F_{\text{Nicotine plus NS9283}}/F_0$ and $\Delta F_{\text{Nicotine}}/F_0$ within the same cell was significant. An unpaired t test with the Welch correction was used to determine whether the extent of NS9283 potentiation was different across different experimental conditions. Parameters were considered different if the p-value was less than 0.05. Graphing and statistical analysis were performed using Prism 8 (GraphPad).

Results

Stoichiometric forms of α4β2 nAChRs distinguished by single-channel current amplitude

We previously established that the two predominant stoichiometric forms of the α4β2 nAChR could be distinguished by their single-channel current amplitudes [26]. Indeed, following co-transfection of equal amounts of α4 and β2 subunit cDNAs into BOSC 23 cells, recordings of ACh-elicited single-channel currents exhibit channel openings with two distinct current amplitudes (Fig. 1a). After measuring the amplitude of each channel opening event and compiling the amplitudes into a histogram, fitting the sum of two Gaussian functions to the histogram reveals two peaks with mean amplitudes of 3.3 and 4.1 pA (Fig. 1b). Previous studies using concatemeric α4β2 nAChRs demonstrated that channel openings with the larger unitary current amplitude arose from receptors with the $(\alpha4)_3(\beta2)_2$ stoichiometry, whereas channel openings with the smaller unitary amplitude arose from receptors with the $(\alpha4)_2(\beta2)_3$ stoichiometry [26]. For the experiment illustrated, the relative areas of the two Gaussian components are similar, and statistical analysis of multiple experiments shows that the relative areas of the two components are not different (Fig. 1c, Table 1). Although the observation of two Gaussian components of current amplitudes indicates the presence of each stoichiometric form, the relative areas do not necessarily indicate the relative amounts of the two forms. The reason is that the two forms differ in their sensitivity to ACh and in their extent of steady-state desensitization. Nevertheless, under conditions of a 1:1 transfection ratio of α4 to β2 subunit cDNAs, each of the two stoichiometric forms is clearly present and functional on the cell surface.

NACHO promotes the $(\alpha4)_2(\beta2)_3$ stoichiometry

Following co-transfection with equal amounts of α4 and β2 subunit cDNAs, plus the cDNA encoding NACHO, recordings of ACh-elicited single-channel currents reveal channel openings with a single predominant current amplitude (Fig. 1d). After measuring the amplitude of each channel opening event and compiling the amplitudes into a histogram, fitting a single Gaussian function to the histogram provides a good fit with a mean current amplitude of 3.25 pA (Fig. 1e). In addition, the standard deviation

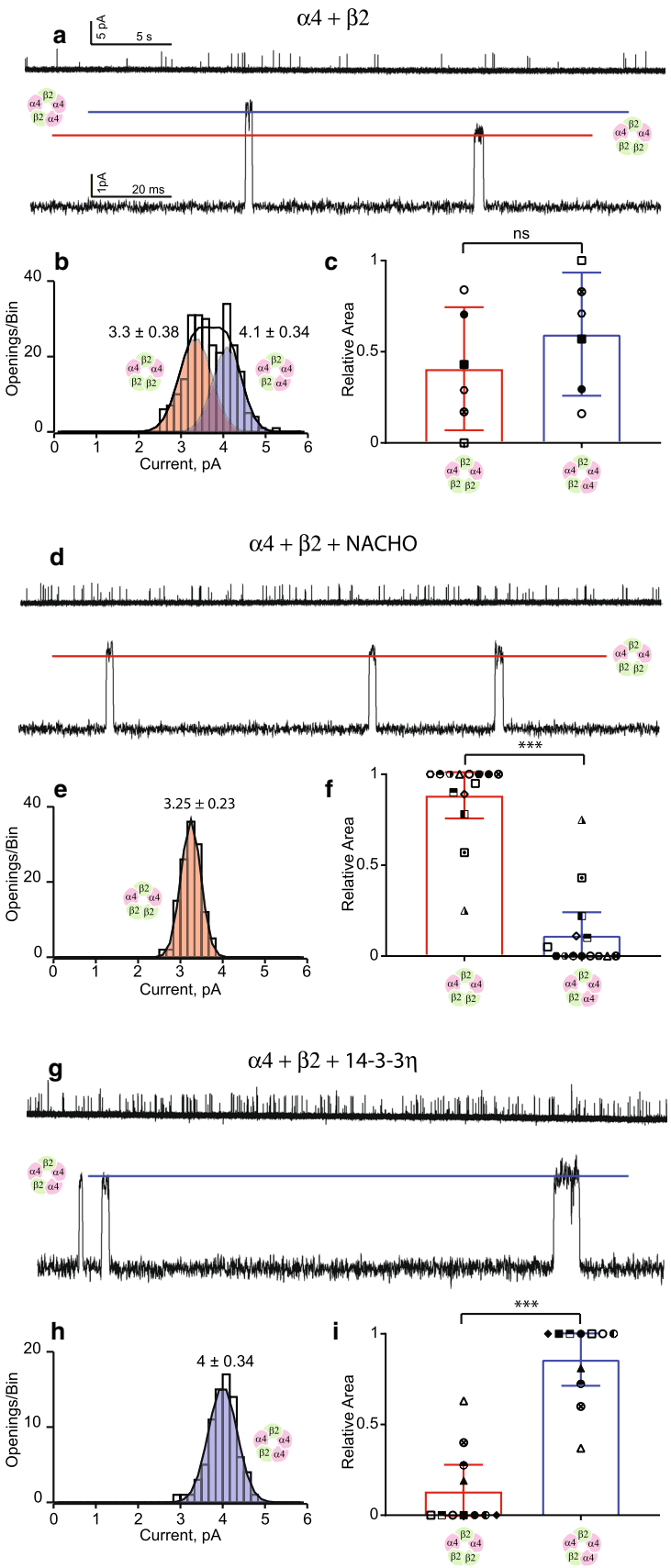

Fig. 1 Stoichiometric forms of α4β2 nAChRs determined by unitary current amplitude. BOSC 23 cells were transfected with α4 and β2 subunits without (**a**–**c**) and either with NACHO (D-F) or 14-3-3η (G-I). Single-channel currents were recorded in the cell-attached patch configuration with a concentration of 10 μM ACh in the pipette and a holding potential of −70 mV. Representative traces with different magnifications are shown for each experimental condition (**a, d, g**). Below the traces is a histogram of detected single-channel currents that reached full amplitude with the indicated means and S.D. of each Gaussian peak (left panels) (**b, e, h**). Mean and 95% CI of the relative areas, along with a statistical comparison of the Gaussian components, are shown for multiple patches (right panel) (**c, f, i**). Measurements from individual patches are indicated with different symbols. Statistical differences are indicated as *** (significantly different, $p < 0.001$) and ns (not significantly different, $p > 0.05$)

Table 1 Single-channel currents amplitudes of $(\alpha4)_2(\beta2)_3$ and $(\alpha4)_3(\beta2)_2$ stoichiometries without and with NACHO or 14-3-3η

Stoichiometric variant	α4 + β2 [1:1] (6 patches; 423 openings)		α4 + β2 + Nacho [1:1:0.3] (14 patches; 1532 openings)		α4 + β2 + 14-3-3η [1:1:1] (18 patches; 705 openings)	
	Amplitude (pA [95% CI])	Area (Weight [95% CI])	Amplitude (pA [95% CI])	Area (Weight [95% CI])	Amplitude (pA [95% CI])	Area (Weight [95% CI])
$(\alpha4)_2(\beta2)_3$	3.2 [3.0; 3.4]	0.41 [0.07; 0.74]	3.3 [3.2; 3.4]	0.88 [0.75; 1]	3.4 [3.16; 3.56]	0.14 [0.009; 0.28]
$(\alpha4)_3(\beta2)_2$	4.0 [3.8; 4.1]	0.59 [0.26-0.93]	4.1 [3.7; 4.4]	0.12 [0.008; 0.24]	4.0 [3.85; 4.09]	0.86 [0.72; 1]
Statistical differences between pairs; $p < 0.05$	Yes; $p < 0.0001$	No; $p = 0.33$	Yes; $p < 0.0001$	Yes; $p < 0.007$	Yes; $p < 0.0001$	Yes; $p < 0.0001$

Amplitudes and fractional areas are given along with 95% CI. Statistical differences in amplitudes and fractional areas between stoichiometric variants and corresponding p-values are shown in the bottom row

of the fitted Gaussian function is somewhat smaller than that for the corresponding component in the absence of either NACHO or 14-3-3η where both receptor stoichiometries were present (Fig. 1b), further indicating a single population of current amplitudes. The results of recordings from multiple patches show that NACHO strongly biases the receptor population toward the stoichiometry with a unitary current amplitude of 3.3 pA (Table 1) and that the prevalence of the small over the large current amplitude is significant (Fig. 1f, Table 1). Thus, NACHO biases the population of functional receptors towards the $(\alpha4)_2(\beta2)_3$ stoichiometry.

14-3-3η promotes the $(\alpha4)_3(\beta2)_2$ stoichiometry

Following co-transfection with equal amounts of α4 and β2 subunit cDNAs, plus the cDNA encoding 14-3-3η, recordings of ACh-elicited single-channel currents reveal channel openings with a single predominant current amplitude (Fig. 1g), but the amplitude is greater than observed with NACHO. After measuring the amplitude of each channel opening episode and compiling the amplitudes into a histogram, a single Gaussian function provides a good fit with a mean amplitude of 4 pA (Fig. 1h). The standard deviation of the fitted Gaussian function is the same as that obtained for the component with the larger current amplitude in absence of either NACHO or 14-3-3η where both receptor stoichiometries were present (Fig. 1b). The results of recordings from multiple patches show that 14-3-3η strongly biases the receptor population toward that with a unitary current amplitude of 4 pA (Table 1) and that the prevalence of the larger over the smaller current amplitude is significant (Fig. 1i, Table 1). Thus, 14-3-3η biases the receptor population towards the $(\alpha4)_3(\beta2)_2$ stoichiometry.

Stoichiometric variants assessed by calcium imaging

In the cell-attached patch mode, the patch-clamp technique monitors functional receptors within a small fraction of the total plasma membrane of the cell. Thus, our conclusions that NACHO and 14-3-3η promote a single stoichiometric variant of the α4β2 nAChR rely on sampling a sufficient number of membrane patches. To monitor functional receptors from the entire cell, we transfected BOSC 23 cells with cDNA encoding GCaMP5G, a cytosolic protein that increases fluorescence upon binding calcium, together with cDNAs encoding α4 and β2 subunits, without or with NACHO or 14-3-3η. We then perfused cells with a solution containing the agonist nicotine and measured the increase in fluorescence within individual cells (Fig. 2a); we chose nicotine as the agonist, rather than ACh, to avoid potential activation of muscarinic AChRs. To distinguish between the two stoichiometric forms, the potentiator NS9283, which selectively potentiates the $(\alpha4)_3(\beta2)_2$ stoichiometry [26, 53], was co-applied with nicotine. A positive difference between the fluorescence elicited by nicotine plus NS9283 and that elicited by nicotine alone indicates the presence of the $(\alpha4)_3(\beta2)_2$ stoichiometry (Fig. 2a).

For an exemplar cell transfected with equal amounts of α4 and β2 subunits, application of nicotine alone elicits a robust fluorescence signal that rises rapidly and decays more slowly (Fig. 2b, left panel). Our patch clamp recordings show that both stoichiometric forms are present under these conditions, and because both forms are permeable to calcium [54], we conclude that the fluorescence signal arises from both stoichiometric forms. After a recovery period in the absence of nicotine, application of nicotine plus NS9283 elicits a fluorescence signal with an amplitude approximately 50% greater than elicited by nicotine alone, with the difference representing the additional calcium influx due to potentiation of the fraction of the receptor population with stoichiometry $(\alpha4)_3(\beta2)_2$ (Fig. 2b, left panel).

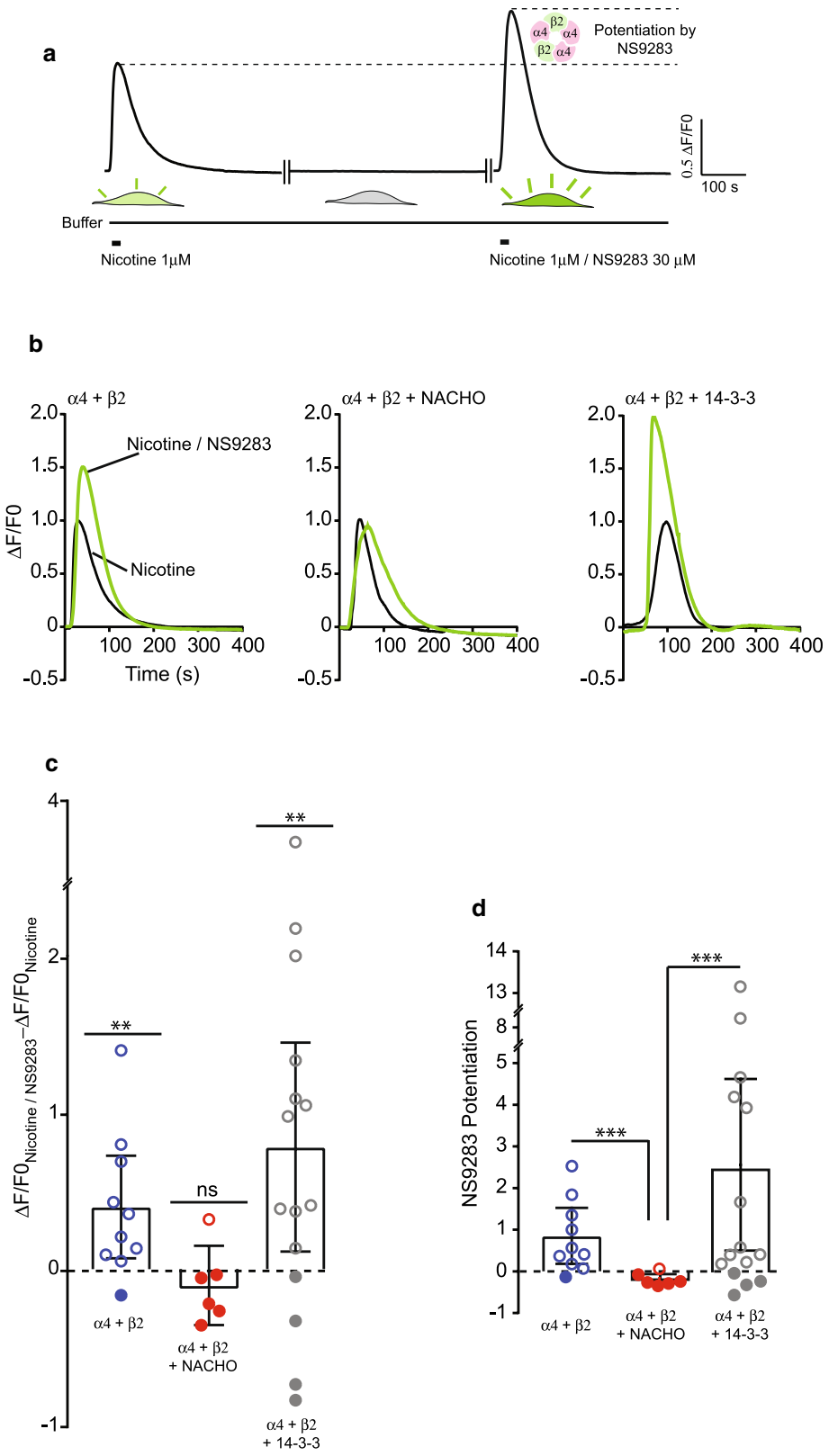

Fig. 2 Stoichiometric forms of α4β2 nAChRs determined by calcium imaging. BOSC 23 cells were transfected with cDNAs encoding GCaMP5G, α4, and β2 subunits, either without or with NACHO or 14-3-3η. Fluorescence changes ($\Delta F/F_0$) in response to nicotine alone followed by nicotine plus NS9283 were recorded from the same cell (**a**). Representative responses to nicotine (black) and nicotine plus NS9283 (green) are overlaid for single-cells expressing α4 and β2 without (**b**, left panel) and with either NACHO (**b**, middle panel) or 14-3-3η (**b**, right panel). Means of the difference between responses to nicotine plus NS9283 and nicotine alone (**c**) and the extent of potentiation by NS9283 (**d**) are shown, with the error bars indicating the 95% CI. Open circles represent responses from cells in which the fluorescence changes indicated potentiation by NS9283, whereas the filled circles represent responses from cells in which the changes indicated no potentiation by NS9283. Statistical differences between the peaks (**c**) and extents of potentiation (**d**) are indicated as *** (significantly different, $p < 0.001$), ** (significantly different, $p < 0.05$) and ns (not significantly different, $p > 0.05$)

For an exemplar cell transfected with equal amounts of α4 and β2 subunits plus NACHO, application of nicotine alone elicits a fluorescence response with an amplitude that is equivalent to that elicited by nicotine plus NS9382 (Fig. 2b, middle panel). The absence of a detectable increase by NS9283 indicates that receptors with stoichiometry

$(\alpha4)_3(\beta2)_2$ are markedly reduced or absent, in agreement with our observation of a single class of receptors with a reduced current amplitude corresponding to the $(\alpha4)_2(\beta2)_3$ stoichiometry (Fig. 1d–f). On the other hand, for an exemplar cell transfected with equal amounts of α4 and β2 subunits plus 14-3-3η, nicotine plus NS9283 elicits a fluorescence increase approximately twice that elicited by nicotine alone (Fig. 2b, right panel). The difference between the two responses is about twice that observed in the absence of either NACHO or 14-3-3η, indicating a population of receptors enriched in the $(\alpha4)_3(\beta2)_2$ stoichiometry.

The compiled results from fluorescence imaging of multiple cells support the results from exemplar cells. Without either NACHO or 14-3-3η, the response to nicotine is greater in the presence of NS9283 than in its absence, and the difference between the two responses is statistically different from zero, confirming the presence of a mixed population of the two stoichiometric forms (Fig. 2c, Table 2). However, with NACHO, the response to nicotine is the same in either the presence or absence of NS9283; the difference between the two responses is not statistically different from zero, confirming the receptor population is enriched in the $(\alpha4)_2(\beta2)_3$ stoichiometry (Table 2). By contrast, with 14-3-3η, the response to nicotine is much greater in the presence of NS9283 than in its absence, and the difference is approximately twice that observed in the absence of 14-3-3η, confirming the receptor population is enriched in the $(\alpha4)_3(\beta2)_2$ stoichiometry (Table 2).

To quantify the extent of potentiation, we computed the ratio of the peak fluorescence increase elicited by nicotine plus NS9283 to that elicited by nicotine alone and subtracted the number one from that ratio (Fig. 2d, Table 2). Without NACHO, the extent of potentiation is ~ 0.8, whereas, with NACHO, the extent of potentiation is not different from zero. Moreover, the extent of potentiation is greater without compared to NACHO. Analogously, with 14-3-3η, the extent of potentiation ranges between 2 and 3, and in some cells is greater than 10, and is greater than that observed with NACHO (Table 2). Thus, results from calcium imaging, which monitors functional receptors from the entire cell, support the results from patch-clamp recording: NACHO biases the receptor population toward the stoichiometric form $(\alpha4)_2(\beta2)_3$, whereas 14-3-3η biases the receptor population toward the form $(\alpha4)_3(\beta2)_2$.

Discussion

The α4β2 nAChR is the most abundant type of nicotinic receptor in the brain and assembles in two predominant stoichiometric forms. The two forms differ dramatically in their sensitivity to ACh and the potentiator NS9283, and they also differ in their regional distributions. While functional differences between the two forms are significant toward synaptic signaling and therapeutics, mechanisms by which the two stoichiometric forms are regulated are equally significant. The chaperones NACHO and 14-3-3η have been shown to increase trafficking of α4β2 nAChRs to the plasma membrane, but whether they alter the balance of the two stoichiometric forms was not known. By exploiting the different single-channel current amplitudes of the two stoichiometric forms, and the selective potentiation of one form by NS9283, we show that NACHO and 14-3-3η have opposing effects on expression of the two stoichiometric forms. In cells transfected with equimolar amounts of cDNAs encoding α4 and β2 subunits, both stoichiometric forms are present and

Table 2 Effect of NACHO and 14-3-3η on the expression of the α4β2 stoichiometries measured by calcium imaging

cDNA transfection ratios	$\Delta F_{Nicotine}/F_0$ [95% CI]	$\Delta F_{Nicotine\ plus\ NS9283}/F_0$ [95% CI]	$\Delta F_{Nicotine\ plus\ NS9283}/F_0$ - $\Delta F_{Nicotine}/F_0$ [95% CI] (Statistical difference between responses to nicotine and nicotine plus NS9283; $p<0.05$)	NS9283 potentiation [95% CI] (Statistical difference between pairs; $p<0.05$)
A: α4 + β2 [1:1] $n=10$	0.63 [0.4; 0.8]	1 [0.7; 1.3]	0.41 [0.08; 0.74] (Yes; $p=0.02$)	+0.82 [0.2; 1.4]
B: α4 + β2 + NACHO [1:1:0.3] $n=6$	1.45 [−0.6; 3.5]	1.36 [−0.9; 3.6]	−0.09 [−0.35; 0.16] (No; $p=0.39$)	−0.19 [−0.4; −0.03] (B vs C, yes; $p=0.02$) (B vs A, yes; $p=0.005$)
C: α4 + β2 + 14-3-3 [10:1:10] $n=15$	1 [0.6; 1.5]	1.84 [1.2; 2.4]	0.79 [0.12; 1.5] (Yes; $p=0.02$)	+2.43 [0.3; 4.6] (C vs A, No; $p=0.14$)

cDNA transfection ratios for α4, β2, NACHO, and 14-3-3η and the number of cells assayed (n) are specified in the left column. For each cell, the change in fluorescence in response to 1 μM nicotine alone ($\Delta F_{Nicotine}/F_0$) followed by 1 μM nicotine plus the stoichiometry-selective potentiator NS9283 ($\Delta F_{Nicotine\ plus\ NS9283}/F_0$) was determined. Means of $\Delta F_{Nicotine}/F_0$ and $\Delta F_{Nicotine\ plus\ NS9283}/F_0$ along with their differences ($\Delta F_{Nicotine\ plus\ NS9283}/F_0 - \Delta F_{Nicotine}/F_0$) and NS9283 potentiation are shown with 95% CI. NS9283 potentiation was defined as the response to nicotine plus NS9283 relative to the response to nicotine alone as: $\left(\left[\frac{\Delta F\text{Nicotine plus NS9283}}{F0}\Big/\frac{\Delta F\text{Nicotine}}{F0}\right]-1\right)$. Statistical differences and p-values are shown in brackets

functional on the cell surface, as shown the presence of two distinct amplitudes of ACh-evoked single-channel currents and the ability of NS9283 to enhance nicotine-evoked calcium uptake. However, in the presence of NACHO, only the smaller of the two amplitude classes of currents is observed, and NS9283 does not enhance nicotine-evoked calcium uptake. Thus, NACHO promotes the $(\alpha4)_2(\beta2)_3$ stoichiometry, and to our knowledge, is the first endogenous protein shown to promote this stoichiometry. On the other hand, in the presence of 14-3-3η, only the larger amplitude class of single-channel currents is observed, and NS9283 markedly enhances nicotine-evoked calcium uptake. Although 14-3-3η has been shown to reduce the ACh sensitivity of α4β2 nAChRs [43], this is the first demonstration at the single-channel level that 14-3-3η promotes the $(\alpha4)_3(\beta2)_2$ stoichiometry. Thus, in addition to the prototoxin Lynx1 [55, 56], 14-3-3η becomes the second endogenous protein shown to promote the $(\alpha4)_3(\beta2)_2$ stoichiometry. The overall results suggest that in pathological conditions such as nicotine dependence and epilepsy, NACHO, 14-3-3η, and their molecular partners are potential drug targets toward rebalancing the subunit stoichiometry of α4β2 AChRs.

Herein the functional consequences of NACHO and 14-3-3η are monitored at the level of fully assembled, functional α4β2 nAChRs on the cell surface, yet both chaperones act intracellularly: NACHO is an ER-resident transmembrane protein [36, 37], whereas 14-3-3η is a cytosolic protein [42]. The action of 14-3-3η on α4β2 nAChRs was discovered by using the large intracellular domain of the α4 subunit as bait in a yeast two-hybrid screen, and the resulting hit was shown to increase steady-state amounts of the α4 subunit within the ER and increase α4β2 nAChRs on the cell surface [42]. Our observation that 14-3-3η enriches cell surface receptors in the $(\alpha4)_3(\beta2)_2$ stoichiometry suggests that 14-3-3η either slows the degradation of the α4 subunit, and by mass action increases the $(\alpha4)_3(\beta2)_2$ stoichiometry, or enhances the ability of the α4 subunit to oligomerize with individual subunits or higher-order assembly intermediates. NACHO was discovered by a genetic screen for the ability to promote expression of functional homomeric α7 nAChRs, which in the absence of chaperones are retained intracellularly. NACHO was also tested on a variety of neurotransmitter activated receptors, revealing that it increased expression of α4β2 nAChRs, as assessed by ACh-elicited macroscopic currents and radiolabeled epibatidine binding [37]. However, whether NACHO affects the stability of α4 or β2 subunits or their ability to form oligomers was not investigated. Our observation that NACHO promotes the $(\alpha4)_2(\beta2)_3$ stoichiometry suggests it either stabilizes the β2 subunit within the ER or enhances its ability to oligomerize with other subunits or assembly intermediates.

Recent ex vivo studies using a genetically encoded fluorescent α4 subunit revealed differences in the regional distributions of the two stoichiometric forms [22]. In addition, immunochemical determination of the ratio of α4 to β2 subunits also revealed differences in regional distributions [21]. The $(\alpha4)_3(\beta2)_2$ stoichiometry is enriched in the cerebral cortex, hippocampus, and cerebellum, whereas the $(\alpha4)_2(\beta2)_3$ stoichiometry predominates in the thalamus [21, 22]. The $(\alpha4)_3(\beta2)_2$ stoichiometry is also enriched in Renshaw cells of the spinal cord [24]. mRNA encoding NACHO is abundant in the cerebral cortex, hippocampus and olfactory bulb [37], whereas 14-3-3η protein is abundant in the cerebral cortex [40]. Thus, physiologically, NACHO and 14-3-3η may fine-tune the two stoichiometric forms, and this interplay may be disrupted in pathological conditions. Future studies of the localization of receptor subunits and chaperone proteins with cellular resolution could potentially test these possibilities.

Previous work showed that nicotine crosses the plasma membrane and affects the assembly of α4β2 nAChRs within the ER and Golgi [32], increasing receptor expression on the cell surface and promoting the $(\alpha4)_2(\beta2)_3$ stoichiometry in vitro [25, 33] and in vivo [21, 22]. Following nicotine administration, a shift from the $(\alpha4)_3(\beta2)_2$ to the $(\alpha4)_2(\beta2)_3$ stoichiometry has also been observed in the cerebral cortex and hippocampus [21, 22]. Interestingly, perinatal nicotine administration increases levels of NACHO protein [57], suggesting that in addition to its direct actions as a pharmacological chaperone, nicotine may also act through NACHO to promote the $(\alpha4)_2(\beta2)_3$ stoichiometry.

Mutations in the genes encoding the α4 and β2 subunits cause Autosomal Dominant Nocturnal Frontal Lobe Epilepsy (ADNFLE) [58]. In vitro studies of ADNFLE mutations, using fluorescence energy transfer methods, showed that a variety of ADNFLE mutations increased the $(\alpha4)_3(\beta2)_2$ stoichiometry and that this increase was countered by nicotine [59]. Nicotine patches or cigarette smoking have also been shown to reduce the incidence of seizures in patients with ADNFLE [60–64]. Thus, NACHO, 14-3-3η and their interacting molecular partners emerge as potential drug targets to reestablish imbalances in the stoichiometry of α4β2 nAChRs caused by ADNFLE mutations.

In summary, our single-channel and calcium imaging measurements show that NACHO and 14-3-3η exert opposing effects in biasing the subunit stoichiometry of functional, cell surface α4β2 nAChRs. The findings have implications toward the physiology of synaptic signaling and the development of therapeutics to rebalance the subunit stoichiometry in pathological conditions involving α4β2 nAChRs.

Authors' contributions Conceptualization: SM, SMS; Methodology: SM, CA; Formal analysis and investigation: SM, STW and CA; Writing—original draft preparation: SM and SMS; Writing—review and

editing: SM, STW, CA, AB and SMS; Funding acquisition: SMS; Resources: AB and SMS; Supervision: SMS.

Funding National Institutes of Health; award number NS31744 to Steven M Sine.

Compliance with ethical standards

Conflict of interest The authors declare that they have no conflict of interest.

References

1. Millar NS, Gotti C (2009) Diversity of vertebrate nicotinic acetylcholine receptors. Neuropharmacology 56:237–246. https://doi.org/10.1016/j.neuropharm.2008.07.041
2. Albuquerque EX, Pereira EFR, Alkondon M, Rogers SW (2009) Mammalian nicotinic acetylcholine receptors: from structure to function. Physiol Rev 89:73–120. https://doi.org/10.1152/physrev.00015.2008
3. Gu Z, Yakel JL (2011) Timing-dependent septal cholinergic induction of dynamic hippocampal synaptic plasticity. Neuron. https://doi.org/10.1016/j.neuron.2011.04.026
4. Dajas-Bailador F, Wonnacott S (2004) Nicotinic acetylcholine receptors and the regulation of neuronal signalling. Trends Pharmacol Sci. https://doi.org/10.1016/j.tips.2004.04.006
5. Gray R, Rajan AS, Radcliffe KA, Yakehiro M, Dani JA (1996) Hippocampal synaptic transmission enhanced by low concentrations of nicotine. Nature 383:713–716. https://doi.org/10.1038/383713a0
6. Sine SM (2012) End-plate acetylcholine receptor: structure, mechanism, pharmacology, and disease. Physiol Rev. https://doi.org/10.1152/physrev.00015.2011
7. Kent L, Middle F, Hawi Z, Fitzgerald M, Gill M, Feehan C et al (2001) Nicotinic acetylcholine receptor α4 subunit gene polymorphism and attention deficit hyperactivity disorder. Psychiatr Genet 11:37–40. https://doi.org/10.1097/00041444-200103000-00007
8. Sarter M, Parikh V, Howe WM (2009) nAChR agonist-induced cognition enhancement: integration of cognitive and neuronal mechanisms. Biochem Pharmacol. https://doi.org/10.1016/j.bcp.2009.04.019
9. Sabri O, Meyer PM, Gräf S, Hesse S, Wilke S, Becker G-A et al (2018) Cognitive correlates of α4β2 nicotinic acetylcholine receptors in mild Alzheimer's dementia. Brain 141:1840–1854. https://doi.org/10.1093/brain/awy099
10. Sun Y, Yang Y, Galvin VC, Yang S, Arnsten AF, Wang M (2017) Nicotinic α4β2 cholinergic receptor influences on dorsolateral prefrontal cortical neuronal firing during a working memory task. J Neurosci 37:5366–5377. https://doi.org/10.1523/JNEUROSCI.0364-17.2017
11. McGranahan TM, Patzlaff NE, Grady SR, Heinemann SF, Booker TK (2011) α4β2 nicotinic acetylcholine receptors on dopaminergic neurons mediate nicotine reward and anxiety relief. J Neurosci 31:10891–10902. https://doi.org/10.1523/JNEUROSCI.0937-11.2011
12. Hurst R, Rollema H, Bertrand D (2013) Nicotinic acetylcholine receptors: from basic science to therapeutics. Pharmacol Ther. https://doi.org/10.1016/j.pharmthera.2012.08.012
13. Laviolette SR, van der Kooy D (2004) The neurobiology of nicotine addiction: bridging the gap from molecules to behaviour. Nat Rev Neurosci 5:55–65. https://doi.org/10.1038/nrn1298
14. Picciotto MR, Kenny PJ (2013) Molecular mechanisms underlying behaviors related to nicotine addiction. Cold Spring Harb Perspect Med. 3:a012112. https://doi.org/10.1101/cshperspect.a012112
15. Taly A, Corringer P-J, Guedin D, Lestage P, Changeux J-P (2009) Nicotinic receptors: allosteric transitions and therapeutic targets in the nervous system. Nat Rev Drug Discov. 8:733–750. https://doi.org/10.1038/nrd2927
16. Zoli M, Pistillo F, Gotti C (2015) Diversity of native nicotinic receptor subtypes in mammalian brain. Neuropharmacology 96:302–311. https://doi.org/10.1016/j.neuropharm.2014.11.003
17. Marubio LM, del Mar Arroyo-Jimenez M, Cordero-Erausquin M, Lena C, Le Novere N, de Kerchove d'Exaerde A et al (1999) Reduced antinociception in mice lacking neuronal nicotinic receptor subunits. Nature 398:805–810. https://doi.org/10.1038/19756
18. Picciotto MR, Zoli M, Léna C, Bessis A, Lallemand Y, LeNovère N et al (1995) Abnormal avoidance learning in mice lacking functional high-affinity nicotine receptor in the brain. Nature 374:65–67. https://doi.org/10.1038/374065a0
19. Ross SA, Wong JY, Clifford JJ, Kinsella A, Massalas JS, Horne MK et al (2000) Phenotypic characterization of an alpha 4 neuronal nicotinic acetylcholine receptor subunit knock-out mouse. J Neurosci 20:6431–6441
20. Zoli M, Léna C, Picciotto MR, Changeux JP (1998) Identification of four classes of brain nicotinic receptors using β mutant mice. J Neurosci 18:4461–4472. https://doi.org/10.1523/jneurosci.18-12-04461.1998
21. Fasoli F, Moretti M, Zoli M, Pistillo F, Crespi A, Clementi F et al (2016) In vivo chronic nicotine exposure differentially and reversibly affects upregulation and stoichiometry of α4β2 nicotinic receptors in cortex and thalamus. Neuropharmacology 108:324–331. https://doi.org/10.1016/j.neuropharm.2016.04.048
22. Fu X, Moonschi FH, Fox-Loe AM, Snell AA, Hopkins DM, Avelar AJ et al (2019) Brain region specific single-molecule fluorescence imaging. Anal Chem 91:10125–10131. https://doi.org/10.1021/acs.analchem.9b02133
23. DeDominicis KE, Sahibzada N, Olson TT, Xiao Y, Wolfe BB, Kellar KJ et al (2017) The (α 4) 3 (β 2) 2 stoichiometry of the nicotinic acetylcholine receptor predominates in the rat motor cortex. Mol Pharmacol 92:327–337. https://doi.org/10.1124/mol.116.106880
24. Lamotte d'Incamps B, Zorbaz T, Dingova D, Krejci E, Ascher P (2018) Stoichiometry of the heteromeric nicotinic receptors of the renshaw cell. J Neurosci 38:4943–4956. https://doi.org/10.1523/jneurosci.0070-18.2018
25. Moroni M, Zwart R, Sher E, Cassels BK, Bermudez I (2006) alpha4beta2 nicotinic receptors with high and low acetylcholine sensitivity: pharmacology, stoichiometry, and sensitivity to long-term exposure to nicotine. Mol Pharmacol 70:755–768. https://doi.org/10.1124/mol.106.023044
26. Mazzaferro S, Bermudez I, Sine SM (2017) α4β2 nicotinic acetylcholine receptors: relationships between subunit stoichiometry and function at the single channel level. J Biol Chem 292:2729–2740. https://doi.org/10.1074/jbc.M116.764183
27. Carbone L, Moroni M, Groot-Kormelink P-J, Bermudez I (2009) Pentameric concatenated (alpha4)(2)(beta2)(3) and (alpha4)(3)(beta2)(2) nicotinic acetylcholine receptors: subunit arrangement determines functional expression. Br J Pharmacol 156:970–981. https://doi.org/10.1111/j.1476-5381.2008.00104.x
28. Walsh RM, Roh SH, Gharpure A, Morales-Perez CL, Teng J, Hibbs RE (2018) Structural principles of distinct assemblies of the human α4β2 nicotinic receptor. Nature 557:261–265. https://doi.org/10.1038/s41586-018-0081-7

29. Morales-Perez CL, Noviello CM, Hibbs RE (2016) Manipulation of subunit stoichiometry in heteromeric membrane proteins. Structure. 24:797–805. https://doi.org/10.1016/j.str.2016.03.004
30. Srinivasan R, Richards CI, Xiao C, Rhee D, Pantoja R, Dougherty D et al (2012) Pharmacological chaperoning of nicotinic acetylcholine receptors reduces the endoplasmic reticulum stress response. Mol Pharmacol 81:759–769. https://doi.org/10.1124/mol.112.077792
31. Lester HA, Xiao C, Srinivasan R, Son CD, Miwa J, Pantoja R et al (2009) Nicotine is a selective pharmacological chaperone of acetylcholine receptor number and stoichiometry. Implications for drug discovery. AAPS J. 11:167–177. https://doi.org/10.1208/s12248-009-9090-7
32. Srinivasan R, Pantoja R, Moss FJ, Mackey EDW, Son CD, Miwa J et al (2011) Nicotine up-regulates alpha4beta2 nicotinic receptors and ER exit sites via stoichiometry-dependent chaperoning. J Gen Physiol 137:59–79. https://doi.org/10.1085/jgp.201010532
33. Nelson ME, Kuryatov A, Choi CH, Zhou Y, Lindstrom J (2003) Alternate stoichiometries of alpha4beta2 nicotinic acetylcholine receptors. Mol Pharmacol 63:332–341
34. Buisson B, Bertrand D (2001) Chronic exposure to nicotine upregulates the human (alpha)4((beta)2 nicotinic acetylcholine receptor function. J Neurosci 21:1819–1829
35. Fox AM, Moonschi FH, Richards CI (2015) The nicotine metabolite, cotinine, alters the assembly and trafficking of a subset of nicotinic acetylcholine receptors. J Biol Chem 290:24403–24412. https://doi.org/10.1074/jbc.M115.661827
36. Matta JA, Gu S, Davini WB, Lord B, Siuda ER, Harrington AW et al (2017) NACHO mediates nicotinic acetylcholine receptor function throughout the brain. Cell Rep. 19:688–696. https://doi.org/10.1016/j.celrep.2017.04.008
37. Gu S, Matta JA, Lord B, Harrington AW, Sutton SW, Davini WB et al (2016) Brain α7 nicotinic acetylcholine receptor assembly requires NACHO. Neuron 89:948–955. https://doi.org/10.1016/j.neuron.2016.01.018
38. Rex EB, Shukla N, Gu S, Bredt D, DiSepio D (2017) A genome-wide arrayed cDNA screen to identify functional modulators of α7 nicotinic acetylcholine receptors. SLAS Discov. 22:155–165. https://doi.org/10.1177/1087057116676086
39. Boston PF, Jackson P, Thompson RJ (1982) Human 14–3-3 protein: radioimmunoassay, tissue distribution, and cerebrospinal fluid levels in patients with neurological disorders. J Neurochem 38:1475–1482. https://doi.org/10.1111/j.1471-4159.1982.tb07928.x
40. Umahara T, Uchihara T, Nakamura A, Iwamoto T (2011) Differential expression of 14-3-3 protein isoforms in developing rat hippocampus, cortex, rostral migratory stream, olfactory bulb, and white matter. Brain Res 1410:1–11. https://doi.org/10.1016/j.brainres.2011.06.036
41. Gu Q, Cuevas E, Raymick J, Kanungo J, Sarkar S (2020) Down-regulation of 14-3-3 proteins in Alzheimer's disease. Mol Neurobiol 57:32–40. https://doi.org/10.1007/s12035-019-01754-y
42. Jeanclos EM, Lin L, Treuil MW, Rao J, DeCoster MA, Anand R (2001) The chaperone protein 14-3-3η interacts with the nicotinic acetylcholine receptor α4 subunit. J Biol Chem 276:28281–28290. https://doi.org/10.1074/JBC.M011549200
43. Exley R, Moroni M, Sasdelli F, Houlihan LM, Lukas RJ, Sher E et al (2006) Chaperone protein 14-3-3 and protein kinase a increase the relative abundance of low agonist sensitivity human α4β2 nicotinic acetylcholine receptors in Xenopus oocytes. J Neurochem 98:876–885. https://doi.org/10.1111/j.1471-4159.2006.03915.x
44. Mazzaferro S, Benallegue N, Carbone A, Gasparri F, Vijayan R, Biggin PC et al (2011) Additional Acetylcholine (ACh) binding site at α4/α4 interface of (α4β2)2α4 nicotinic receptor influences agonist sensitivity. J Biol Chem 286:31043–31054. https://doi.org/10.1074/jbc.M111.262014
45. Lee BS, Gunn RB, Kopito RR (1991) Functional differences among nonerythroid anion exchangers expressed in a transfected human cell line. J Biol Chem 266(18):11448–11454
46. Pear WS, Nolan GP, Scott ML, Baltimore D (1993) Production of high-titer helper-free retroviruses by transient transfection. Proc Natl Acad Sci USA 90:8392–8396
47. Sine SM (1993) Molecular dissection of subunit interfaces in the acetylcholine receptor: identification of residues that determine curare selectivity. Proc Natl Acad Sci USA 90:9436–9440
48. Sine SM, Quiram P, Papanikolaou F, Kreienkamp HJ, Taylor P (1994) Conserved tyrosines in the alpha subunit of the nicotinic acetylcholine receptor stabilize quaternary ammonium groups of agonists and curariform antagonists. J Biol Chem 269:8808–8816
49. Mazzaferro S, Bermudez I, Sine SM (2019) Potentiation of a neuronal nicotinic receptor via pseudo-agonist site. Cell Mol Life Sci. https://doi.org/10.1007/s00018-018-2993-7
50. Sine SM, Claudio T, Sigworth FJ (1990) Activation of Torpedo acetylcholine receptors expressed in mouse fibroblasts. Single channel current kinetics reveal distinct agonist binding affinities. J Gen Physiol 96:395–437
51. Mukhtasimova N, DaCosta CJB, Sine SM (2016) Improved resolution of single channel dwell times reveals mechanisms of binding, priming, and gating in muscle AChR. J Gen Physiol 148:43–63. https://doi.org/10.1085/jgp.201611584
52. Colquhoun D, Sigworth FL (1983) Fitting and statistical analysis of single channel records single channel recording. Springer, Boston, pp 483–587. https://doi.org/10.1007/978-1-4615-7858-1_11
53. Timmermann DB, Sandager-Nielsen K, Dyhring T, Smith M, Jacobsen A-M, Nielsen EØ et al (2012) Augmentation of cognitive function by NS9283, a stoichiometry-dependent positive allosteric modulator of α2- and α4-containing nicotinic acetylcholine receptors. Br J Pharmacol 167:164–182. https://doi.org/10.1111/j.1476-5381.2012.01989.x
54. Tapia L, Kuryatov A, Lindstrom J (2007) Ca^{2+} permeability of the (alpha4)3(beta2)2 stoichiometry greatly exceeds that of (alpha4)2(beta2)3 human acetylcholine receptors. Mol Pharmacol 71:769–776. https://doi.org/10.1124/mol.106.030445
55. Nichols WA, Henderson BJ, Yu C, Parker RL, Richards CI, Lester HA et al (2014) Lynx1 shifts α4β2 nicotinic receptor subunit stoichiometry by affecting assembly in the endoplasmic reticulum. J Biol Chem 289:31423–31432. https://doi.org/10.1074/jbc.M114.573667
56. Ibañez-Tallon I, Miwa JM, Wang HL, Adams NC, Crabtree GW, Sine SM et al (2002) Novel modulation of neuronal nicotinic acetylcholine receptors by association with the endogenous prototoxin lynx1. Neuron 33:893–903. https://doi.org/10.1016/S0896-6273(02)00632-3
57. Wichern F, Jensen MM, Christensen DZ, Mikkelsen JD, Gondré-Lewis MC, Thomsen MS (2017) Perinatal nicotine treatment induces transient increases in NACHO protein levels in the rat frontal cortex. Neuroscience. https://doi.org/10.1016/j.neuroscience.2017.01.026
58. Tinuper P, Bisulli F (2011) Autosomal dominant nocturnal frontal lobe epilepsy. In: Shorvon SD, Andermann F, Guerrini R (eds) The causes of epilepsy. Cambridge University Press, Cambridge, pp 70–73. https://doi.org/10.1017/cbo9780511921001.010
59. Son CD, Moss FJ, Cohen BN, Lester HA (2009) Nicotine normalizes intracellular subunit stoichiometry of nicotinic receptors carrying mutations linked to autosomal dominant nocturnal frontal lobe epilepsy. Mol Pharmacol 75:1137–1148. https://doi.org/10.1124/mol.108.054494

60. Pavlakis PP, Douglass LM (2015) Pearls & Oy-sters: a case of refractory nocturnal seizures: putting out fires without smoke. Neurology. 84:e134–e136. https://doi.org/10.1212/WNL.0000000000001539
61. Willoughby JO, Pope KJ, Eaton V (2003) Nicotine as an antiepileptic agent in ADNFLE: an N-of-one study. Epilepsia. 44:1238–1240. https://doi.org/10.1046/j.1528-1157.2003.58102.x-i1
62. Ghasemi M, Hadipour-Niktarash A (2015) Pathologic role of neuronal nicotinic acetylcholine receptors in epileptic disorders: implication for pharmacological interventions. Rev Neurosci 26(2):199–223
63. Lossius K, de Saint Martin A, Myren-Svelstad S, Bjørnvold M, Minken G, Seegmuller C et al (2020) Remarkable effect of transdermal nicotine in children with CHRNA4-related autosomal dominant sleep-related hypermotor epilepsy. Epilepsy Behav 105:106944. https://doi.org/10.1016/j.yebeh.2020.106944
64. Brodtkorb E, Picard F (2006) Tobacco habits modulate autosomal dominant nocturnal frontal lobe epilepsy. Epilepsy Behav 9:515–520. https://doi.org/10.1016/j.yebeh.2006.07.008

Publisher's Note Springer Nature remains neutral with regard to jurisdictional claims in published maps and institutional affiliations.